High-order harmonic generation by two linearly polarized laser fields with an arbitrary angle between their polarization axes

D. Habibović [1], W. Becker [2] and D. B. Milošević [1,3,2,*]

[1] *University of Sarajevo, Faculty of Science, Zmaja od Bosne 35, 71000 Sarajevo, Bosnia and Herzegovina*

[2] *Max-Born-Institut for Nonlinear Optics and Short Pulse Spectroscopy, Max-Born-Strasse 2a, 12489 Berlin, Germany*

[3] *Academy of Sciences and Arts of Bosnia and Herzegovina, Bistrik 7, 71000 Sarajevo, Bosnia and Herzegovina*

(Received 23 May 2022; revised 13 July 2022; accepted 19 August 2022; published 30 August 2022)

High-order harmonic generation by two linearly polarized fields that enclose an arbitrary crossing angle θ is investigated using the strong-field approximation. We investigate the combinations with frequency ratios $s/r = 2$ and 3 with integer r and s. In the former case, the emitted harmonics are elliptically polarized unless $\theta = 0^\circ$ or 90°, while in the latter they are always elliptically polarized except for $\theta = 0^\circ$. The possibility to control the intensity and ellipticity of the emitted harmonics by variation of the relative phase φ between the field components and the crossing angle θ is explored. There are regions with large harmonic ellipticity and appreciable intensity in the relative-phase–harmonic-order plane and they are more extended for values of the crossing angle closer to 90°. The overall shape of the spectra (smooth, oscillatory, or erratic) for different values of θ and φ is explained using the saddle-point method and quantum-orbit theory. The simple-man model is utilized to assess the regions with large harmonic intensity and to predict the position of the cutoff. For the frequency ratio $s/r = 2$, the harmonic ellipticity is significant even for extremely small deviations of the crossing angle θ from 90°.

DOI: 10.1103/PhysRevA.106.023119

I. INTRODUCTION

An atom exposed to a strong laser field radiates harmonics of the fundamental field through the process called high-order harmonic generation (HHG) (see, for example, the review article [1] and references therein). In this process, the electron is liberated from the parent atom and propagates under the influence of the laser field and the potential of its parent ion. If the laser field is strong enough, the effect of the latter on the propagation can be neglected so that the electron can be described by a Volkov state. Since the laser field oscillates in time, the electron may return to the parent ion and recombine. The energy gained from the laser field plus the ionization potential is released in the form of a high-energy photon. Depending on the parameters of the driving field, this radiation can extend into the vacuum ultraviolet, extreme ultraviolet, and even soft-x-ray spectral regions and it lends itself to various applications. Alternative methods to obtain electromagnetic radiation in these spectral regions include x-ray lasers, synchrotron radiation, or free-electron lasers, all of which exceed the facilities of smaller research laboratories.

The tunability of the light obtained in the HHG process has allowed investigations of many different systems. For example, soft x rays provide unique capabilities for probing materials because they can penetrate an opaque material without disturbing its structure. Also, there is an inherent sensitivity to the composition of the material and its chemical or magnetic state [2–5]. Furthermore, because of their short wavelength, coherent beams allow a microscopy that can image at the wavelength limit in three dimensions and, because of their high frequencies, any relevant dynamics can be captured [6–9]. Finally, elliptically polarized harmonics are particularly important for the study of molecular chiral properties. For example, in Refs. [10,11] circularly polarized light was employed to induce enantioselective photoionization of unoriented chiral molecules. High-order harmonics obtained by an elliptically polarized pulse were used to measure the photoelectron circular dichroism of chiral molecules [12], and in Ref. [13] it was shown theoretically that the photoelectron circular dichroism can be accessed using two linearly polarized fields with mutually orthogonal polarizations. Chiral harmonic generation was implemented relying on the comparatively weak magnetic component of an elliptically polarized driving pulse [14]. A scenario employing only electric dipole interactions was proposed by Ayuso *et al.* [15].

The HHG process can be controlled using the laser-field parameters, so it is advantageous to have as many of them as possible. If a monochromatic plane-wave laser field is used as the driving field, the available parameters are its intensity, ellipticity, and wavelength. However, if a two-component laser field is employed many other parameters become available. Examples are the intensities, ellipticities, and wavelengths of the field components, as well as their relative phase. The characteristics of the HHG spectra can be radically different when a two-component field is employed as the driving field. Particularly interesting is the bicircular field, which consists of two coplanar counterrotating circularly polarized fields. In this case the harmonics are circularly polarized and the helicity of adjacent harmonics is opposite [16,17]. Another configuration that has become popular in recent years is the

*Corresponding author: milo@bih.net.ba

orthogonally polarized two-color (OTC) field, which consists of two mutually orthogonal linearly polarized components with frequencies that are integer multiples of a fundamental frequency ω. The first experimental results with this field were obtained many years ago [17–19]. For the ω-2ω configuration, both odd and even harmonics are emitted and they are linearly polarized [odd (even) in the direction of the ω (2ω) component]. For the ω-3ω field, only odd harmonics having elliptical polarization appear in the spectrum. The influence of the relative phase on the harmonic spectra generated by an OTC field was analyzed in Refs. [20–22] and the conclusions obtained were confirmed in Refs. [23–33]. More recently, time-dependent density-functional theory was employed to study HHG in an OTC field [34], and a method to retrieve the temporal intensity profile of an extreme ultraviolet attosecond pulse was discussed in Ref. [35]. Also, harmonic emission was analyzed experimentally for molecular targets exposed to an OTC field [36], and harmonic emission from oriented CO molecules exposed to the same field was investigated in [37]. In Ref. [38], using the time-dependent Schrödinger equation, HHG induced by a polarization-skewed laser pulse was investigated where the polarization of each driving cycle points in a different direction. Inhomogeneous OTC fields were used for control of the polarization direction of an isolated attosecond pulse [39]. Finally, spatial molecular interferometry via multidimensional high-harmonic spectroscopy by an OTC field was considered in [40].

Generalization of the OTC field to an arbitrary crossing angle between the two laser-field components has also attracted attention. In principle, this angle can easily be controlled in experiments. For example, in Ref. [41] the photoelectron momentum distribution of argon atoms was analyzed using a field configuration with a crossing angle of 45°. Also, using a similar configuration with an arbitrary crossing angle, in Refs. [42,43] it was shown that the harmonic ellipticity can be controlled using the crossing angle and the relative phase as control knobs. Finally, we mention that the laser-field components can also be elliptically polarized. In this case, their ellipticity can serve as another control parameter. The HHG process for this configuration was extensively analyzed in Refs. [44,45]. Moreover, using the same field configuration, Ref. [46] demonstrated that HHG is sensitive to the shape of the atomic potential well and the size of the valence orbitals. A linearly polarized fundamental with an elliptically polarized second harmonic superimposed can be used for efficient molecular orientation [47]. The combination of linearly and circularly polarized fields was employed to study the electronic subcycle dynamics [48], and field components having small ellipticity were used to produce an attosecond pulse train [49].

In the past we analyzed high-order harmonic spectra obtained exposing an atom to various laser-field configurations using a theory based on the strong-field approximation (SFA). This is much less time consuming than the solution of the time-dependent Schrödinger equation. The SFA assumes that the influence of the ionic potential is negligible during the propagation of the electron in the continuum. For example, encouraged by the experimental results [50], we applied this theory to HHG in a bichromatic elliptically polarized laser field with special emphasis on the bicircular field [51–53]. The selection rules were obtained for atoms with closed and nonclosed shells using the projection of the total angular momentum on the quantization axis, and the difference between harmonic emission for atoms with s and p ground states was explored. Moreover, in Refs. [54,55] HHG induced by an OTC field was investigated. In particular, it was shown that for the ω-3ω OTC field the emitted harmonics are elliptically polarized and that their ellipticity can be controlled by changing the intensities of the field components as well as the relative phase. The possibility of using this field configuration for the production of an attosecond pulse was analyzed in Ref. [56]. In contrast, the harmonics produced by the ω-2ω OTC field are always linearly polarized. The general case of a bichromatic elliptically polarized laser field was analyzed [44], but still the angle between the laser-field components was 90°. A systematic derivation of the selection rules for atomic and molecular targets exposed to various laser fields can be found in Ref. [57], and a similar derivation based on group theory is given in Ref. [58]. Finally, a theoretical method that combines time-dependent effective-range theory and the quasienergy formalism has been extended to driving pulses of arbitrary shape in Refs. [59,60]. This includes bicircular and OTC fields with arbitrary pulse lengths.

In this paper we analyze the case where HHG is induced by two linearly polarized fields with an arbitrary angle in between their polarizations. This angle is a new parameter which, together with the other laser parameters, can be used to control the harmonic intensity and the harmonic ellipticity. The article is organized as follows. In Sec. II we define the laser field and briefly present the SFA theory that we will utilize. Also, we discuss the saddle-point method and the simple-man model. In Sec. III we present and discuss our numerical results. In Sec. IV we present our conclusions together with a brief outlook. Atomic units are used throughout the article unless otherwise stated.

II. THEORY

We explore the HHG process induced by a two-component laser field, with the electric field vector $\mathbf{E}(t) = (E_x(t), E_y(t))$ given by

$$\begin{aligned} E_x(t) &= E_1 \sin(r\omega t) + E_2 \cos\theta \sin(s\omega t + \varphi), \\ E_y(t) &= E_2 \sin\theta \sin(s\omega t + \varphi), \end{aligned} \tag{1}$$

where $I_j = E_j^2$ $(j = 1, 2)$ are the intensities of the field components, ω is the fundamental frequency, r and s are integers, and φ is the relative phase. The field components are linearly polarized, one in the x direction and the other in the direction at the angle θ with respect to the x direction. For example, for $\theta = 90°$ the field (1) is an OTC field, while for $\theta = 0°$ it is a bichromatic linearly polarized field. Examples of this field, for several values of the relative phase and $\theta = 30°$, are presented in Fig. 1, where polar plots of the electric field (black solid lines) and the corresponding vector potential $\mathbf{A}(t) = -\int^t \mathbf{E}(t')dt'$ (red dashed lines) are shown for the ω-2ω [Figs. 1(a)–1(c)] and ω-3ω [Figs. 1(d)–1(f)] configurations. The arrows indicate the direction of the time evolution.

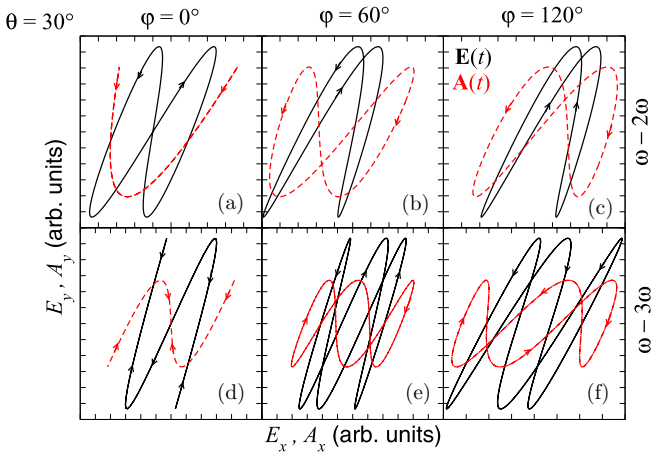

FIG. 1. Electric field (black solid lines) and the corresponding vector potential (red dashed lines) of the two-component field (1) for $\theta = 30^\circ$ and (a)–(c) $(r, s) = (1, 2)$ and (d)–(f) $(r, s) = (1, 3)$. The relative phase is (a) and (d) $\varphi = 0^\circ$, (b) and (e) $\varphi = 60^\circ$, and (c) and (f) $\varphi = 120^\circ$. The direction of the time evolution is indicated by arrows. The intensities of the field components are equal.

A. Strong-field approximation

For a laser field with period $T = 2\pi/\omega$, the intensity of the nth harmonic is [61,62]

$$P_n = \frac{(n\omega)^4}{2\pi c^3}|\mathbf{T}_n|^2, \tag{2}$$

where $\mathbf{T}_n$ is the T-matrix element, which can be written as the Fourier component of the time-dependent dipole

$$\mathbf{T}_n = \int_0^T \frac{dt}{T}\sum_m \mathbf{d}_m(t)e^{in\omega t}. \tag{3}$$

The sum over m is the sum over all possible values of the magnetic quantum number m of the atomic ground state (we consider atoms with closed electron shells so that the magnetic quantum number of the initial and final state is the same, as it was explained in [53]). We assume that the time-dependent dipole, the Fourier transform of which yields the harmonic-emission spectrum, is the coherent sum (3). In [53] it was argued that this is appropriate for multielectron atoms. This theory was successfully applied to explain the conservation of the spin angular momentum [52]. The harmonic ellipticity can be obtained using the numerically calculated components of the vector $\mathbf{T}_n$ and the relations [44]

$$\varepsilon_n = \mathrm{sgn}(\xi_n)\sqrt{\frac{1-\sqrt{1-\xi_n^2}}{1+\sqrt{1-\xi_n^2}}}, \quad \xi_n = \frac{\mathrm{Im}(2T_{nx}^* T_{ny})}{|\mathbf{T}_n|^2}. \tag{4}$$

In the SFA, the time-dependent dipole is [53,61]

$$\mathbf{d}_m(t) = -i\left(\frac{2\pi}{i}\right)^{3/2}\int_0^\infty \frac{d\tau}{\tau^{3/2}}\langle\psi_m|\mathbf{r}|\mathbf{k}_{\mathrm{st}} + \mathbf{A}(t)\rangle \times e^{iS(\mathbf{k}_{\mathrm{st}};t_0,t)}\langle\mathbf{k}_{\mathrm{st}} + \mathbf{A}(t_0)|\mathbf{r}\cdot\mathbf{E}(t_0)|\psi_m\rangle, \tag{5}$$

where $|\psi_m\rangle$ is the ground-state atomic wave function, $\mathbf{k}_{\mathrm{st}}(t_0, t) = -\int_{t_0}^t dt'\mathbf{A}(t')/\tau$ is the stationary momentum, $S(\mathbf{k}_{\mathrm{st}}; t_0, t) = -\int_{t_0}^t dt'[\mathbf{k}_{\mathrm{st}} + \mathbf{A}(t')]^2/2 - I_p\tau$ is the action, I_p is the ionization potential, and t_0, t, and $\tau = t - t_0$ are the ionization, recombination, and the so-called travel time, respectively. For atoms with an s ground state, such as He, the magnetic quantum number is zero, while for atoms with a p ground state such as Ne the possible values of the magnetic quantum number are $m = 0, \pm 1$. The influence of spin is not taken into consideration. The atomic ground state is modeled by a linear combination of Slater-type orbitals $\psi_{n_alm} \propto r^{n_a-1}e^{-\zeta_a r}Y_{lm}(\Omega)$, with $n_a = 2$ and $l = 1$ [63], in the same way it was done in [53]. The magnetic quantum numbers of the initial and final states are the same because the electron liberated from a state with one value of this quantum number cannot end up in some other state because it is already occupied by other electrons. Following the procedure presented in Ref. [57], it is easy to check that both odd and even harmonics are emitted when the ω-2ω field drives the process, while for the ω-3ω field only odd harmonics are expected in the spectra regardless of the value of the crossing angle θ. The main advantage of an arbitrary crossing angle is that (unless $\theta = 0^\circ$ or 90°) the emitted harmonics are always elliptically polarized and we expect that the ellipticity can be controlled using the crossing angle as a control parameter. Our theory does not account for Coulomb effects, which can affect the harmonic intensity and ellipticity quantitatively. The theory is developed for long laser pulses with a flat envelope. If the laser-pulse duration used is longer than ten optical cycles, few-cycle-pulse and carrier-envelope-phase effects can usually be neglected [64]. Note that we suppose that propagation effects are small, which is the case when low-pressure gases are used to generate the high harmonics. Otherwise, the high-energy part of the spectrum is strongly suppressed, so only the low-energy part is of interest [65]. Finally, we mention that our theory neglects the self-consistent dynamic electron-electron interaction, which allows one to explain the resonantly enhanced HHG associated with the transfer of energy from the returning electron to the other electrons of the atom [66,67]. Also, the model cannot describe the polarization of atoms, which can affect the probability of ionization from different orbitals [68].

B. Saddle-point method

The harmonic intensity given by Eq. (2) with Eqs. (3) and (5) can be evaluated using the saddle-point method [69–72]. The stationarity conditions $\partial S(\mathbf{k}_{\mathrm{st}}; t_0, t)/\partial t_0 = 0$ and $\partial[S(\mathbf{k}_{\mathrm{st}}; t_0, t) + n\omega t]/\partial t = 0$ lead to the system of equations

$$[\mathbf{k}_{\mathrm{st}} + \mathbf{A}(t_0)]^2 = -2I_p, \quad [\mathbf{k}_{\mathrm{st}} + \mathbf{A}(t)]^2 = 2(n\omega - I_p), \tag{6}$$

which express energy conservation at the times of ionization and recombination. Due to the negative value of $-2I_p$ on the right-hand side of the first equation, these times are complex. The T-matrix element is given by the sum of the contributions of the relevant solutions t_{0s} and t_s of the saddle-point equations

$$\mathbf{T}_n \propto \sum_s \frac{e^{in\omega t_s}}{\tau_s^{3/2}}e^{iS(\mathbf{k}_{\mathrm{st}};t_{0s},t_s)}\mathcal{M}(\mathbf{k}_{\mathrm{st}}; t_{0s}, t_s), \tag{7}$$

where $\mathcal{M}(\mathbf{k}_{\mathrm{st}}; t_{0s}, t_s)$ is the product of the ionization and recombination matrix elements which appear in Eq. (5). The electron trajectories (quantum orbits) and velocities are solutions of Newton's equation of motion $\ddot{\mathbf{r}}(t) = -\mathbf{E}(t)$ with

initial conditions at the complex time t_{0s} and are given by [72]

$$\mathbf{r}(t) = \mathrm{Re}\left[\int_{t_{0s}}^{t} \mathbf{A}(t')dt' + (t - t_{0s})\mathbf{k}_{\mathrm{st}}\right],$$
$$\mathbf{v}(t) = \mathrm{Re}[\mathbf{k}_{\mathrm{st}} + \mathbf{A}(t)], \tag{8}$$

as functions of the real time $t \in [\mathrm{Re}t_{0s}, \mathrm{Re}t_s]$.

C. Simple-man model

Finally, we briefly discuss the two-dimensional simple-man model. The one-dimensional formulation was given in Refs. [73–76], while a generalization to the two-component OTC field can be found in [54]. There is a crucial difference between the simple-man model for a linearly polarized field and for a field that unfolds in a plane: In one dimension, if the electron starts with zero velocity, for any start time (within certain ranges) there is at least one return time. When, however, the electron is driven in a plane, only exceptional start times allow for an exact return. Otherwise, if the electron is to return for an arbitrary start time, it has to depart with a well-defined nonzero initial momentum. This exponentially reduces the weight of the contribution of this start time [69]. Hence, those exceptional start times where the initial momentum is zero are expected to yield the dominant contributions. The two-dimensional simple-man model finds these start times and the corresponding recombination times. Note that if the field nontrivially depends on some parameter such as the relative phase φ, then these times will also depend on this parameter. This mechanism is also embedded in the closed real trajectories of Refs. [59,60].

The motion of the electron in the laser field is described by Newton's equation of motion $\ddot{\mathbf{r}}(t) = -\mathbf{E}(t)$ with the solution

$$\mathbf{r}(t) = \mathbf{r}(t_0) + [\mathbf{v}(t_0) - \mathbf{A}(t_0)](t - t_0) + \int_{t_0}^{t} \mathbf{A}(t')dt', \tag{9}$$

where $\mathbf{r}(t_0)$ and $\mathbf{v}(t_0)$ are the initial position and the initial velocity, respectively, while the kinetic energy just before the recombination at time t is

$$E_k(t_0, t) = \tfrac{1}{2}[\mathbf{k}_{\mathrm{st}}(t_0, t) + \mathbf{A}(t)]^2, \tag{10}$$

with $\mathbf{k}_{\mathrm{st}}(t_0, t) = -\int_{t_0}^{t} dt'\mathbf{A}(t')/(t - t_0)$. Since, as mentioned, the ionization probability exponentially decreases with increasing initial kinetic energy of the photoelectron [69,77], the highest harmonic-emission rate can be expected for $\mathbf{v}(t_0) = \mathbf{0}$. The corresponding harmonic is [54]

$$n_{\mathrm{opt}}\omega = I_p + \tfrac{1}{2}[\mathbf{A}(t) - \mathbf{A}(t_0)]^2 \tag{11}$$

and the pertinent ionization and recombination times are determined by the vector equation

$$\mathbf{k}_{\mathrm{st}}(t_0, t) + \mathbf{A}(t_0) = \mathbf{0}. \tag{12}$$

On the other hand, the maximal harmonic order can be determined by requiring that the electron trajectory be extremal with respect to the kinetic energy, i.e., $\partial E_k(t_0, t)/\partial t_0 = 0$ and $\partial E_k(t_0, t)/\partial t = 0$. These requirements lead to the system of equations

$$[\mathbf{k}_{\mathrm{st}} + \mathbf{A}(t)] \cdot [\mathbf{k}_{\mathrm{st}} + \mathbf{A}(t_0)] = 0,$$
$$[\mathbf{k}_{\mathrm{st}} + \mathbf{A}(t)] \cdot [\mathbf{k}_{\mathrm{st}} + \mathbf{A}(t) + \mathbf{E}(t)\tau] = 0. \tag{13}$$

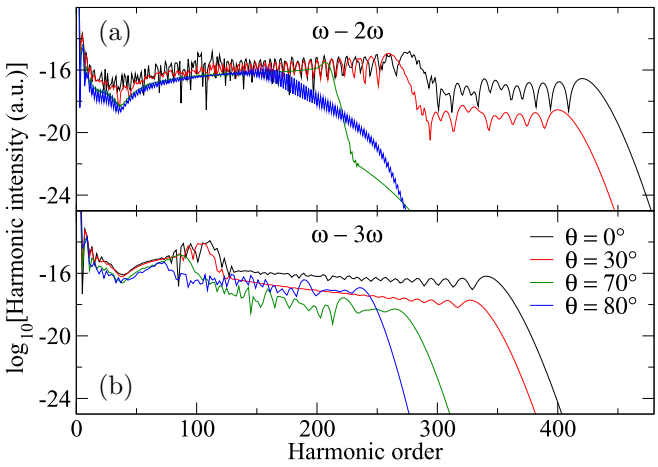

FIG. 2. Logarithm of the harmonic intensity of the Ne atom exposed to the (a) ω-2ω and (b) ω-3ω fields for several values of the crossing angle as indicated in (b). The intensities of the field components are equal, $I_1 = I_2 = 4 \times 10^{14}$ W/cm^2, and the fundamental wavelength and the relative phase are $\lambda = 1300$ nm and $\varphi = 0°$, respectively.

Using the solutions (t_{0m}, t_m) of this system, the maximal harmonic energy is $I_p + E_{km}$, where

$$E_{km} = \tfrac{1}{2}[\mathbf{k}_{\mathrm{st}}(t_{0m}, t_m) + \mathbf{A}(t_m)]^2. \tag{14}$$

III. NUMERICAL RESULTS

In this section we present our numerical results for the Ne atom. The corresponding ionization potential is $I_p = 21.56$ eV. The Ne atom has a p ground state and harmonics with larger ellipticity than in the case of atoms with an s ground state can be expected [53].

A. Control of the harmonic-emission process

We start by investigating the dependence of the harmonic spectra on the crossing angle. In Fig. 2 we present the harmonic intensities for the ω-2ω [Fig. 2(a)] and ω-3ω [Fig. 2(b)] fields for several values of the crossing angle. The intensities of the field components are equal, $I_1 = I_2 = 4 \times 10^{14}$ W/cm^2, the fundamental wavelength is $\lambda = 1300$ nm, and the relative phase $\varphi = 0°$. The spectra obtained using the ω-2ω field strongly depend on the value of the crossing angle. For a bichromatic linearly polarized field (i.e., for $\theta = 0°$) the harmonic spectrum has two plateaus: The first one corresponds to the low- and medium-energy photons, while the second one with a significantly lower harmonic intensity accounts for the high-energy photons. The presence of two well-defined plateaus was noticed in Ref. [78] and explained in Ref. [79] using the semiclassical trajectories of the returning electron. Increasing the value of the crossing angle reduces the yield and the cutoff of the second plateau, while the first one also becomes shorter but with its intensity approximately unchanged. For values of the crossing angle larger than $\theta \approx 60°$ the second plateau is practically absent, while the first maintains its intensity but assumes an unusual shape. For example, for $\theta = 70°$ the harmonic spectrum is very smooth, indicating that only one quantum orbit makes

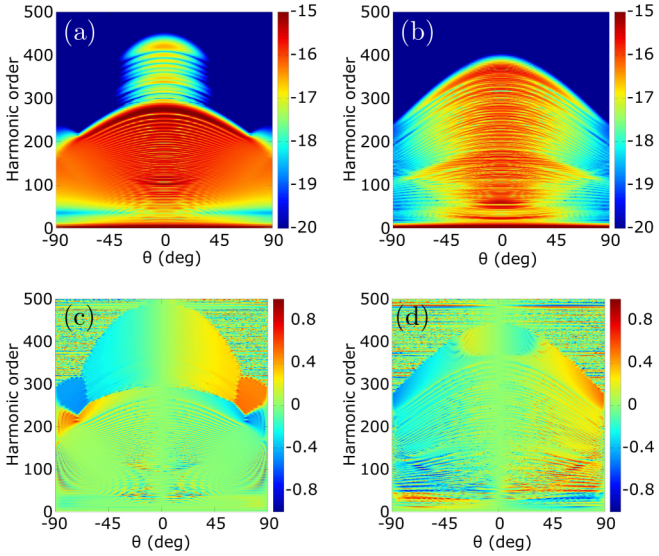

FIG. 3. Logarithm of the (a) and (b) harmonic intensity and (c) and (d) harmonic ellipticity as a function of the crossing angle and the harmonic order for the Ne atom and the ω-2ω field with the relative phase (a) and (c) $\varphi = 0^\circ$ and (b) and (d) $\varphi = 120^\circ$. The other field parameters are the same as in Fig. 2.

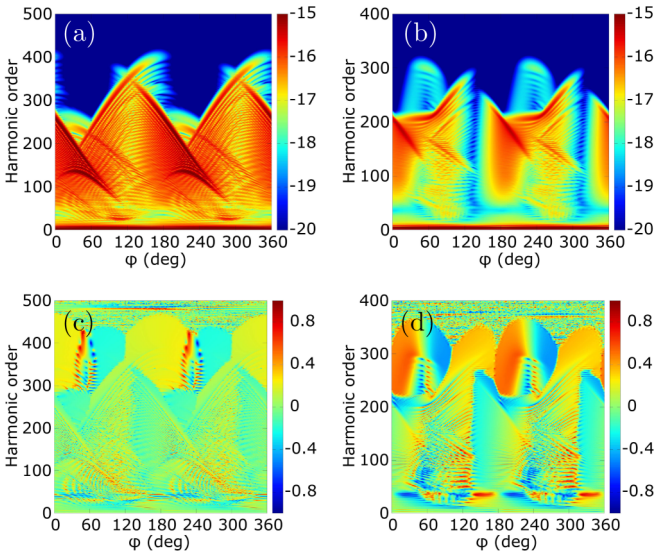

FIG. 4. Logarithm of the (a) and (b) harmonic intensity and (c) and (d) harmonic ellipticity as a function of the relative phase and the harmonic order for the Ne atom exposed to the ω-2ω field with the crossing angles (a) and (c) $\theta = 30^\circ$ and (b) and (d) $\theta = 70^\circ$. The other field parameters are the same as in Fig. 2.

a significant contribution, while for $\theta = 80^\circ$ it looks similar to the spectrum of an OTC field [54,55]. The main difference with respect to the OTC field is that the harmonics are elliptically polarized for all crossing angles except $\theta = 0^\circ$ and 90°. For the ω-3ω field the situation is very different. Only one plateau is present regardless of the value of the crossing angle. As the former increases the plateau becomes shorter, while the harmonic intensity first decreases and then again increases. For example, the intensity of the plateau is similar for $\theta = 30^\circ$ and $\theta = 80^\circ$. Also, for any value of the crossing angle, only odd harmonics are emitted and they are elliptically polarized.

For a more detailed view of the dependence of the harmonic intensity and ellipticity on the crossing angle θ, in Fig. 3 we present the logarithm of the harmonic intensity [Figs. 3(a) and 3(b)] and harmonic ellipticity [Figs. 3(c) and 3(d)] for the Ne atom exposed to the ω-2ω field with the relative phases $\varphi = 0^\circ$ [Figs. 3(a) and 3(c)] and $\varphi = 120^\circ$ [Figs. 3(b) and 3(d)]. The harmonic intensities are unchanged upon $\theta \to -\theta$, while the ellipticity changes its sign. For the limiting case of the OTC field ($\theta = \pm 90^\circ$), for the relative phase $\varphi = 120^\circ$ the harmonics are strongly suppressed (see the left panels of Fig. 1 in [55]). For $\varphi = 0^\circ$ and $-30 < \theta < 30^\circ$, Fig. 3(a) exhibits the second plateau, which we noticed in Fig. 2(a). The θ dependence of the harmonic intensity is different for the relative phases $\varphi = 0^\circ$ and $\varphi = 120^\circ$. The position of the cutoff is strongly dependent on the relative phase and generally highest for $\theta \approx 0^\circ$. For $\theta = \pm 90^\circ$ and $\varphi = 120^\circ$, harmonic emission is very weak except for the very lowest orders.

When the two polarizations become parallel, the harmonic polarization gradually becomes linear, as it should. We know from the selection rules that for the OTC field the harmonics are linearly polarized too, but this is hardly visible in Figs. 3(c) and 3(d) because the transition to zero ellipticity occurs extremely rapidly (discussed in more detail below).

For some regions of the harmonic order and the crossing angle, especially for $\varphi = 120^\circ$, the harmonic intensities fluctuate rapidly as a function of the harmonic order. This behavior has been observed for both atomic and molecular targets [44,55,80,81], but the effect is more pronounced for atomic targets. In addition, the oscillations are particularly noticeable for the ω-2ω field because generally odd and even harmonics have different harmonic ellipticity. Large ellipticities are mostly restricted to parameter regions where the harmonic intensity is low.

Next we will explore the harmonic intensity as a function of the relative phase for fixed crossing angle. Figure 4 displays the logarithm of the harmonic intensity [Figs. 4(a) and 4(b)] and the harmonic ellipticity [Figs. 4(c) and 4(d)] as a function of the relative phase and the harmonic order for the Ne atom and the ω-2ω field with the crossing angles $\theta = 30^\circ$ [Figs. 4(a) and 4(c)] and $\theta = 70^\circ$ [Figs. 4(b) and 4(d)]. As they should, the harmonic spectra are invariant with respect to the transformation $\varphi \to \varphi + 180^\circ$.

For $\theta = 30^\circ$ [Fig. 4(a)] the harmonic spectra have one or two plateaus depending on the value of the relative phase. In general, the second plateau (at higher orders) is weaker, i.e., the harmonic intensity is lower than for the first plateau. For $\theta = 70^\circ$, the plot looks quite different and more varied. For most values of the harmonic order and the relative phase (but not for all), the harmonic intensity is lower than for $\theta = 30^\circ$. Moreover, the entire harmonic intensity is strongly quenched for phases $130^\circ \lesssim \varphi \lesssim 150^\circ$. For phases $50^\circ \lesssim \varphi \lesssim 120^\circ$ the harmonic intensity fluctuates rather erratically as a function of the harmonic order, while it changes only smoothly for $0^\circ < \varphi \lesssim 50^\circ$. Also, around $\varphi = 60^\circ$ the second plateau appears with very low intensity. The emitted harmonics are

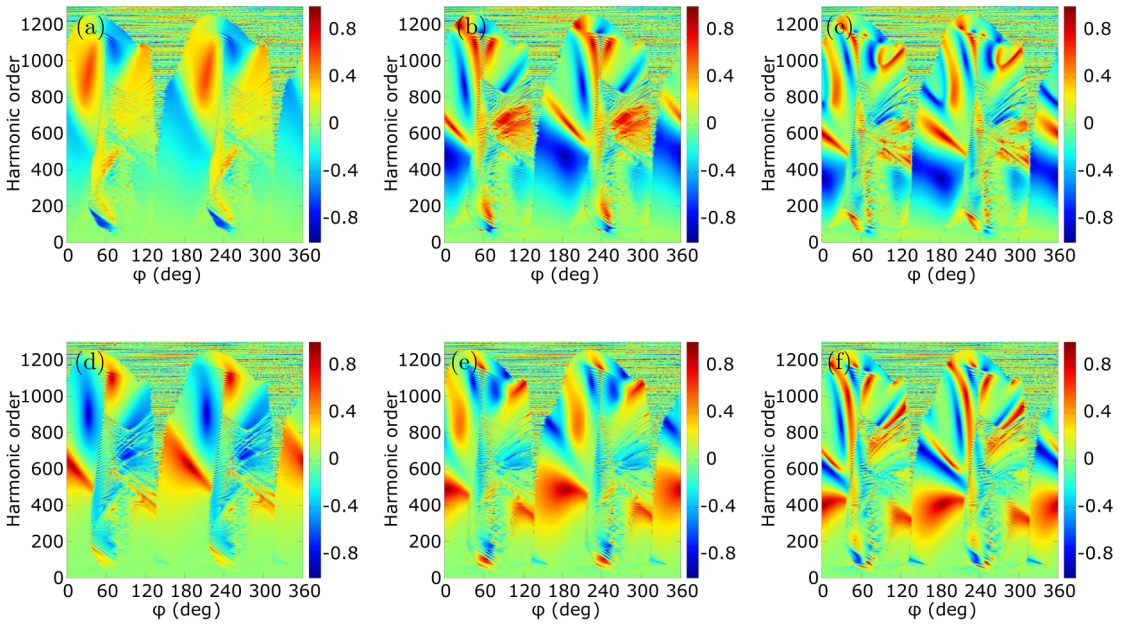

FIG. 5. Ellipticity of the (a)–(c) odd and (d)–(f) even harmonics obtained by exposing a Ne atom to the ω-2ω field with a fundamental wavelength of 2200 nm as a function of the relative phase and harmonic order for the crossing angles (a) and (d) $\theta = 89.9^\circ$, (b) and (e) $\theta = 89.7^\circ$, and (c) and (f) $\theta = 89.5^\circ$. The other field parameters are the same as in Fig. 2.

elliptically polarized regardless of the value of the crossing angle. However, the regions with significant ellipticity in the relative phase-harmonic order plane are broader for $\theta = 70^\circ$ than for $\theta = 30^\circ$ [see Figs. 4(c) and 4(d)]. For $\theta = 70^\circ$, the region around $n = 200$ and $\varphi = 0^\circ$ looks particularly promising in the sense that the ellipticity of the emitted harmonics is large, while the harmonic intensity is still significant. For the ω-2ω field, a particularly interesting situation occurs for crossing angles close to $\theta = 90^\circ$, i.e., close to the OTC field. Namely, for $\theta = 90^\circ$ the harmonics are strictly linearly polarized, while for any other value the polarization is elliptical. The transition occurs extremely rapidly, in complete contrast to what happens when the crossing angle starts deviating from $\theta = 0^\circ$. In Fig. 5 we present the ellipticity of the harmonics obtained by exposing a Ne atom to the ω-2ω field with the fundamental wavelength of 2200 nm as a function of the relative phase and harmonic order for the crossing angles $\theta = 89.9^\circ$ [Figs. 5(a) and 5(d)], $\theta = 89.7^\circ$ [Figs. 5(b) and 5(e)], and $\theta = 89.5^\circ$ [Figs. 5(c) and 5(f)]. Figures 5(a)–5(c) and 5(d)–5(f) correspond to the odd and even harmonics, respectively. The ellipticity observes the symmetry $\varphi \to \varphi + 180^\circ$, as it should. At $\theta = 90^\circ$, even and odd harmonics are linearly polarized, with their polarization directions orthogonal. We can see how this symmetry is immediately broken as the crossing angle starts deviating from 90°. Let us concentrate on relative phases around $\varphi = 180^\circ$ for which the harmonic intensity is a smooth function of the harmonic order. For the crossing angle $\theta = 89.9^\circ$ two regions with large ellipticity appear [see Figs. 5(a) and 5(d)]. Generally, for odd and even harmonics the helicities are opposite, i.e., the harmonics closer to the cutoff have positive (negative) helicity for odd (even) harmonics. In addition, the even harmonics have larger ellipticities, which can become significant even for the smallest deviation from $\theta = 90^\circ$. As the crossing angle decreases, additional regions with large ellipticity appear. In particular, for the crossing angle $\theta = 89.7^\circ$ two additional regions with significant ellipticity appear [see Figs. 5(b) and 5(e)]. Again, the helicity has the opposite sign for odd and even harmonics. With the crossing angle further decreasing, more regions with large ellipticity appear. Formally, a large value of the harmonic ellipticity can be explained in a similar way as for the bielliptical orthogonally polarized field where, for $\theta = 90^\circ$, the harmonics immediately acquire elliptical polarization as soon as the driving fields become ever so slightly elliptically polarized [44].

For a closer look, in Fig. 6 we present the ellipticity of the odd [Fig. 6(a)] and even [Fig. 6(b)] harmonics generated using the same field as in Fig. 5 for the same three crossing angles

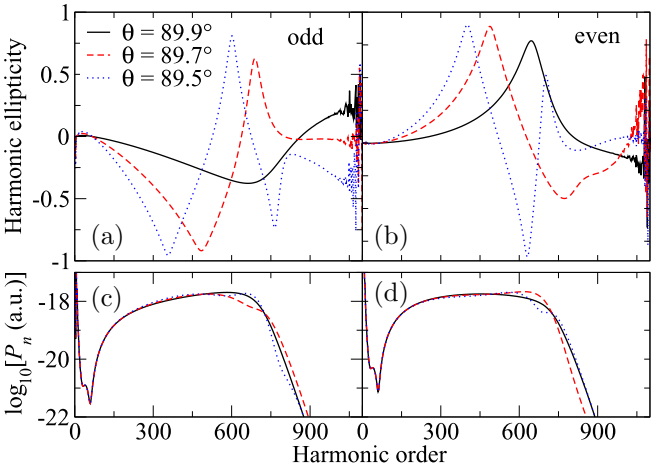

FIG. 6. Harmonic (a) and (b) ellipticity and (c) and (d) intensity of the (a) and (c) odd and (b) and (d) even harmonics obtained by exposing the Ne atom to the same field and for the same crossing angles as in Fig. 5. The relative phase is $\varphi = 180^\circ$.

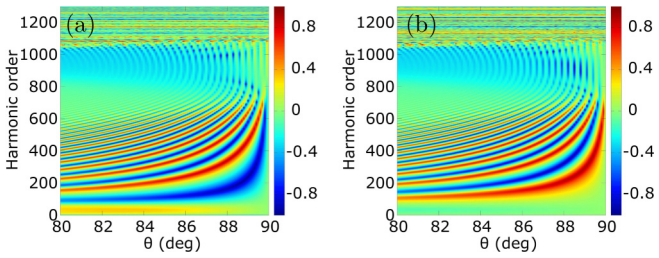

FIG. 7. Harmonic ellipticity of the (a) odd and (b) even harmonics as a function of the crossing angle and harmonic order for the Ne atom exposed to the same field as in Fig. 5. The relative phase is $\varphi = 180^\circ$.

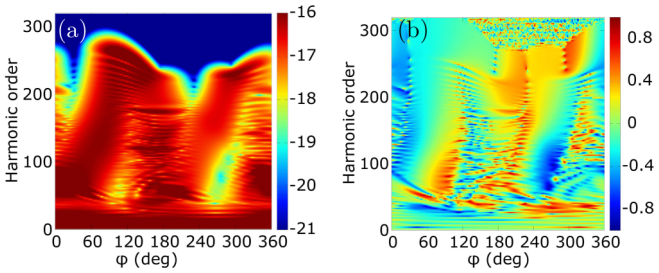

FIG. 8. Logarithm of (a) the harmonic intensity and (b) the harmonic ellipticity as a function of the relative phase and the harmonic order for the Ne atom exposed to the ω-3ω field with the crossing angle $\theta = 80^\circ$. The other field parameters are the same as in Fig. 2.

and for the relative phase $\varphi = 180^\circ$. For $\theta = 89.9^\circ$, the odd harmonics are elliptically polarized with negative helicity all the way up to the cutoff (around $n = 700$) where the ellipticity starts increasing and ultimately changes its sign. However, the corresponding harmonic intensity is already quite low before the cutoff. The even harmonics exhibit similar behavior with the ellipticity having the opposite sign. With decreasing crossing angle, the ellipticity changes its sign twice (for $\theta = 89.7^\circ$) and three times (for $\theta = 89.5^\circ$) before the cutoff. Notice that the harmonic intensities are practically independent of the harmonic order [Figs. 6(c) and 6(d)], while the polarization goes back and forth between linear and almost circular with opposite helicities.

If the crossing angle continues to decrease, the number of oscillations in the harmonic ellipticity continues to increase. This is illustrated in Fig. 7 for $80^\circ \leqslant \theta \leqslant 90^\circ$ and $\varphi = 180^\circ$. This behavior is similar to the observations in Ref. [44] for the bielliptical OTC field (cf. Fig. 10 in Ref. [44]). Now the deviation of the crossing angle from the value $\theta = 90^\circ$ is the source of the breaking of the dynamical symmetry, while in Ref. [44] it was broken by the field components acquiring ellipticity. In order to explain this in more detail we write the vector $\mathbf{T}_n$ given by Eq. (3) as $\mathbf{T}_n = T_n\mathbf{e}_n = T_{n+}\mathbf{e}_+ + T_{n-}\mathbf{e}_-$, where $\mathbf{e}_n$ is the complex unit polarization vector of the nth harmonic, while T_{n+} and T_{n-} are the components with helicities $+1$ and -1, respectively, and $\mathbf{e}_\pm = (\mathbf{e}_x \pm i\mathbf{e}_y)/\sqrt{2}$. The time-dependent dipole $\mathbf{d}_m(t)$, which appears in the vector $\mathbf{T}_n$, contains the matrix element $\langle\psi_{m_f}|\mathbf{r}|\mathbf{q}\rangle = -i\partial\psi_{m_f}(\mathbf{q})/\partial\mathbf{q}$ and the wave function of the final bound state for the Ne atom satisfies the relation $\partial\psi_{m_f}(\mathbf{q})/\partial\mathbf{q} = \partial\psi_{m_f}(\mathbf{q})/\partial q\mathbf{e}_\mathbf{q} + q^{-1}\partial\psi_{m_f}(\mathbf{q})/\partial\theta_q\mathbf{e}_{\theta_q}$, where $\mathbf{q} = \mathbf{k}_{\rm st} + \mathbf{A}(t)$ and, in spherical coordinates, $\mathbf{e}_\mathbf{q} = (\cos\phi_\mathbf{q}, \sin\phi_\mathbf{q}, 0)$ and $\mathbf{e}_{\theta_q} = (-\sin\phi_\mathbf{q}, \cos\phi_\mathbf{q}, 0)$. Using $\mathbf{e}_\pm \cdot \mathbf{e}_\pm = 0$ and $\mathbf{e}_\pm \cdot \mathbf{e}_\mp = 1$, the components of the T-matrix element can be written in the form

$$T_{n\pm} = \mathbf{T}_n \cdot \mathbf{e}_\mp \propto \int dt \int d\tau [f(t,\tau)e^{\mp i\phi_\mathbf{q}(t,\tau)} + g(t,\tau)e^{\pm i\phi_\mathbf{q}(t,\tau)}]. \quad (15)$$

The functions $f(t,\tau)$ and $g(t,\tau)$ are the same for both components of the T-matrix element. The exponential terms contain $\phi_\mathbf{q}(t,\tau)$ and we integrate over t and τ. The function $\phi_\mathbf{q}(t,\tau)$ depends to a great extent on the chosen field configuration, so small deviations of the crossing angle from 90° can lead to a large difference between T_{n+} and T_{n-} and thus harmonics with large ellipticity (recall that the parameter ξ_n [Eq. (4)] can be written as $\xi_n = (|T_{n+}|^2 - |T_{n-}|^2)/(|T_{n+}|^2 + |T_{n-}|^2)$). Finally, we note that again the helicities of the odd and even harmonics are opposite.

The situation is completely different for the ω-3ω OTC field where the harmonics are elliptically polarized regardless of the value of the crossing angle (provided, of course, that it is nonzero, $\theta \neq 0^\circ$). In this case, the ellipticity changes smoothly as a function of the angle θ and the harmonic spectra are not invariant with respect to the transformation $\varphi \to \varphi + 180^\circ$. As an example, in Fig. 8 we present the logarithm of the harmonic intensity [Fig. 8(a)] and the harmonic ellipticity [Fig. 8(b)] as a function of the relative phase and the harmonic order for the Ne atom exposed to the ω-3ω field with the crossing angle $\theta = 80^\circ$. There are extended regions with large ellipticity. For example, for the relative phase around $\varphi = 30^\circ$, the entire region between $n = 80$ and $n = 150$ corresponds to harmonics with large ellipticity and substantial intensity. The regions with large ellipticity become narrower with decreasing crossing angle and when $\theta < 50^\circ$ the ellipticity remains large only for isolated harmonics (not shown). Regions with significant ellipticity can also be found in the low-energy part of the spectra. This is important because the medium- and high-energy harmonics may be suppressed by macroscopic effects [65]. Examples of these regions can be found for really low harmonics, with n around 31 and $0 \leqslant \varphi \leqslant 100$ and $220 \leqslant \varphi \leqslant 350$. For an illustration, in Fig. 9 we present the logarithm of the harmonic intensity (left ordinate) and the harmonic ellipticity (right ordinate) as a function of the harmonic order for the relative phases $\varphi = 45^\circ$ (black solid line) and $\varphi = 320^\circ$ (red dashed line) and the other field parameters the same as in Fig. 8. The harmonic ellipticity can be large even for harmonics with $n < 101$ and their intensities are significant. These regions could be particularly interesting for experiments.

In conclusion, both the ω-2ω and the ω-3ω field configurations generate elliptically polarized harmonics. Regions with significant ellipticity may exist in all parts of the harmonic spectrum depending on the values of the relative phase and the crossing angle, even for crossing angles very close to $\theta = 90^\circ$. Recall that for the ω-2ω field the harmonics have to be linearly polarized if the field components are exactly perpendicular. This transition to linear polarization occurs extremely fast.

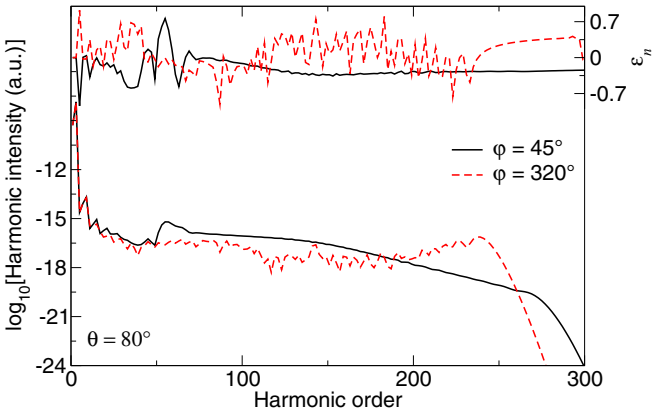

FIG. 9. Logarithm of the harmonic intensity (left ordinate) and the harmonic ellipticity (right ordinate) as functions of the harmonic order for the Ne atom exposed to the same field as in Fig. 8 for the relative phases $\varphi = 45^\circ$ (black solid line) and $\varphi = 320^\circ$ (red dashed line).

B. Saddle-point method

In this section we apply the saddle-point method to explain some features of the HHG spectra. For this purpose, in Fig. 10 we employ the ω-2ω field with the component intensities $I_1 = 2 \times 10^{14}$ W/cm^2, $I_2 = 0.3I_1$, fundamental wavelength $\lambda = 1300$ nm, and the relative phase $\varphi = 0^\circ$. In Fig. 10(a) we present the logarithm of the harmonic intensity as a function of the harmonic order for various values of the crossing angle calculated with the SFA. Both odd and even harmonics are emitted and their intensities begin to differ significantly when the crossing angle approaches 90°. For the OTC field this difference reaches more than an order of magnitude [see the black line in Fig. 10(a)], while for $\theta = 75^\circ$ it is small. Let us now analyze the partial saddle-point contributions to the harmonic yield. The solutions of the saddle-point equations (6) are classified by the multi-index (α, β, m) similarly to the case of a linearly polarized field [82]. For a bichromatic field this classification should be generalized as was done for the bicircular field in [72], but for the laser-field parameters of the present paper the (α, β, m) classification serves its purpose. In Fig. 10(b) we exhibit four partial saddle-point contributions (β, m) to the harmonic yield. The contributions with $\alpha = \pm 1$ are represented by solid and dashed lines. They have different colors for different values of the crossing angle, which correspond to Fig. 10(a). The longer quantum orbits (i.e., those having longer travel times), which contribute to the harmonics with lower energy, are suppressed and only one quantum orbit is enough to reproduce the entire harmonic spectrum. This is the orbit $(-1, 0)$. Only for $\theta = 75^\circ$ does the orbit (1,1) become competitive for the low-energy harmonics. The shape of the SFA spectrum is reproduced well by the saddle-point method. It is smooth when the contribution of only one quantum orbit is significant, while it oscillates or fluctuates if more than one orbit has to be taken into account. The shape of the spectrum is particularly well reproduced for $\theta = 75^\circ$ because in this case the harmonic intensities of adjacent harmonics are similar. We notice that the fact that almost the entire spectrum is dominated by one orbit is unique for the OTC field and also for crossing angles that are not too far away from 90°.

The quantum orbits and the corresponding electron velocities can now be obtained using Eq. (8). In Fig. 11 we present the electric-field vector of the laser field [Fig. 11(a)] and its vector potential [Fig. 11(c)] together with the quantum orbit [Fig. 11(b)] and the electron's velocity [Fig. 11(d)], which correspond to $(\beta, m) = (-1, 0)$. The crossing angle is $\theta = 75^\circ$, while the other field parameters are the same as in Fig. 10. The figures show that the electron is released a few atomic units away from the ion at the moment when the field is close to its maximal value. Thereafter, the electron moves away from the ion following an almost linear trajectory. Eventually, it turns around and returns to the ion following almost the same trajectory. In Fig. 11 the ionization (recombination) times are marked by I (R). Figure 11(d) shows that the electron starts its orbit with a nonzero velocity $\mathbf{v}_0$ in the negative y direction. It is relatively small, so the corresponding harmonic intensity is high because the ionization probability decreases exponentially with $\mathbf{v}_0^2$ [69,77]. In addition, other useful information

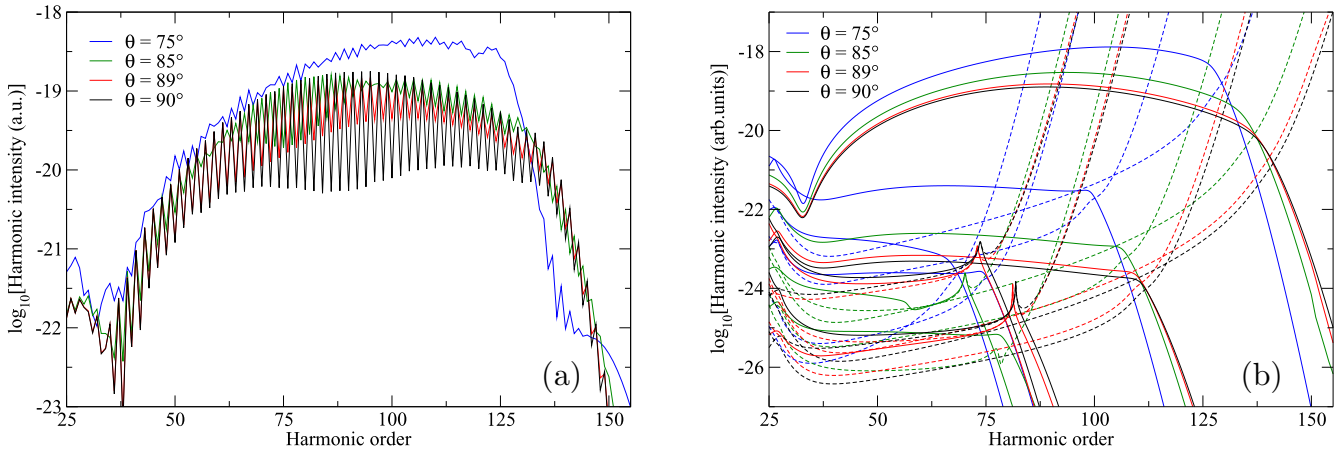

FIG. 10. Logarithm of the harmonic intensity as a function of the harmonic order calculated using (a) the SFA and (b) the saddle-point method for the Ne atom exposed to the ω-2ω field with the crossing angle as given in the legends. The contributions of the solutions represented by the dashed lines have to be disregarded after the cutoff. The intensities of the field components are $I_1 = 2 \times 10^{14}$ W/cm^2 and $I_2 = 0.3I_1$; the fundamental wavelength and the relative phase are the same as in Fig. 2.

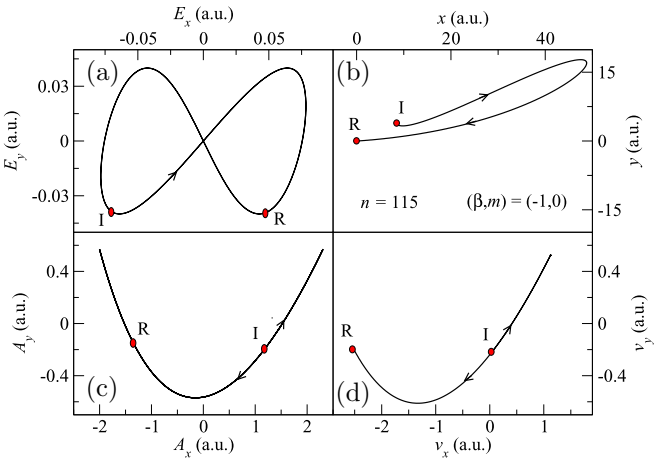

FIG. 11. (a) Electric-field vector and (c) vector potential for the crossing angle $\theta = 75^\circ$. The other laser-field parameters are the same as in Fig. 10. Also shown are (b) the electron trajectory and (d) the velocity between the ionization (I) and recombination (R) times for the harmonic order $n = 115$ and the orbit $(\beta, m) = (-1, 0)$.

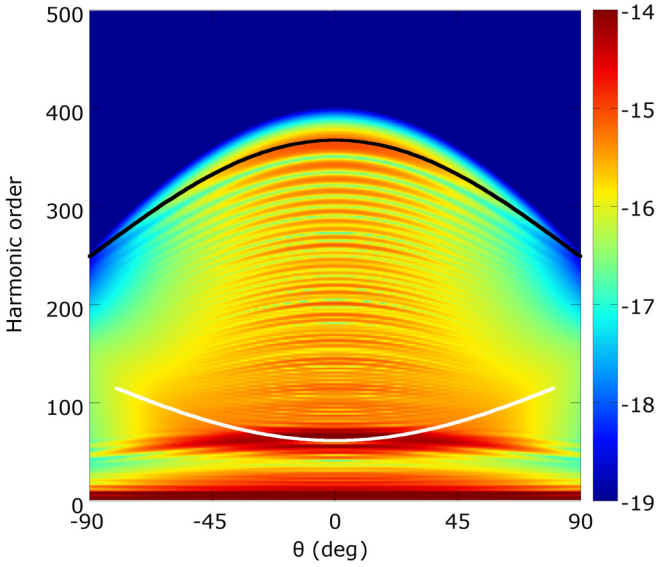

FIG. 12. Logarithm of the harmonic intensity as a function of the crossing angle and harmonic order for the Ne atom exposed to the ω-3ω field with the relative phase $\varphi = 60^\circ$. The black (white) line corresponds to the classical simple-man estimate of the maximal harmonic order (harmonic intensity). The other field parameters are the same as in Fig. 2.

can be extracted from Fig. 11. For example, the electric field at the ionization time is strong, so the ionization probability is significant. Also, the vector potential at the recombination time is large, which leads to a high-energy harmonic photon.

C. Simple-man model

After analyzing the HHG process using the SFA theory as well as the saddle-point method, in this section we analyze the applicability of our simple-man model formulated in Sec. II C to assess the position of the cutoff and the regions with large harmonic intensity. For an illustration, we use the example of the Ne atom and the ω-3ω field. We explore the harmonic intensity as a function of the crossing angle and harmonic order for a fixed value of the relative phase φ. In Fig. 12 we present the logarithm of the harmonic intensity as a function of the crossing angle and the harmonic order for the relative phase $\varphi = 60^\circ$. The black line corresponds to the classical estimate of the position of the cutoff. This classical result agrees very well with the results of the numerical integration. On the other hand, the white line corresponds to the maximal harmonic intensity. Within the region $-45^\circ < \theta < 45^\circ$, this line, which was obtained analytically, satisfactorily predicts the harmonic orders where the intensity is highest as $n \approx 61$. It seems that, for this value of the relative phase, the simple-man model can be used to assess the regions with large harmonic intensity and the position of the cutoff for different values of the crossing angle.

IV. CONCLUSION

The process of high-order harmonic generation allows one to produce elliptically polarized light in the vacuum ultraviolet, extreme ultraviolet, and soft-x-ray spectral regions in a table-top setup. This light has important applications in many branches of science. A linearly polarized laser field generates only linearly polarized harmonics so that two-dimensional fields have to be employed in order to produce elliptical polarization. A bicircular field, which has been analyzed extensively over the past decade, produces only circularly polarized harmonics in the limit of long pulse duration. For short pulses, harmonics with arbitrary ellipticity can be generated [83]. Additionally, to generate elliptically polarized light with tunable ellipticity, other types of tailored laser fields are also suitable [44,54]. Recently, orthogonally polarized two-color laser fields, which consist of two linearly polarized fields with frequencies that are integer multiples of a fundamental frequency and mutually orthogonal polarizations, have attracted a great deal of attention. However, even in this case the emitted harmonics are elliptically polarized only for certain frequency combinations of the laser-field components. A particular problem is that the ω-2ω combination, which can be most easily realized in an experiment, supports only linearly polarized harmonics. This statement only holds for exact orthogonality (see the discussion below).

In this paper we have analyzed a configuration that consists of two linearly polarized fields with an arbitrary crossing angle in between their polarizations. In this case, the emitted harmonics are elliptically polarized regardless of the frequencies of the field components provided the two components are neither parallel nor perpendicular. To calculate the harmonic intensity and the harmonic ellipticity we have used the strong-field approximation and the saddle-point method.

First, we explored how the value of the crossing angle affects the HHG spectrum. We found that the length of the plateau and the harmonic intensity depend to a great extent on this parameter. This dependence is more pronounced for the ω-2ω than for the ω-3ω field combination. For a complete picture, the effect of the crossing angle has to be analyzed along with the relative phase between the field components. For the ω-2ω configuration, the spectrum may consist of one

or two plateaus or the harmonic intensity may be suppressed for all but the lowest-order harmonics, depending on the crossing angle and the relative phase. The emitted harmonics are elliptically polarized. Larger regions with large ellipticity in the plane defined by the relative phase and the harmonic order may exist, especially for crossing angles larger than $\theta \approx 65^\circ$. This has been experimentally confirmed in Ref. [42]. These regions exist in the low-, medium-, and high-energy parts of the harmonic spectra.

The crossing angle and the relative phase also affect the general shape of the spectra. For some values of these parameters the spectrum exhibits an oscillatory or an erratic structure, while for others it is smooth. This is explained with the help of the saddle-point method and quantum-orbit theory. Namely, the shape of the spectrum is related to the number of contributing quantum orbits. If only one quantum orbit plays a role, the spectrum is smooth. For two closely competing quantum orbits, a regular oscillation results, while many contributing orbits generate an erratic behavior of the spectrum. In the saddle-point method, the harmonic order is a continuous parameter. If the difference between the intensities of subsequent odd and even harmonics is large and the contribution of only one quantum orbit is dominant, then the saddle-point method and quantum-orbit theory reproduce the average of the exact SFA results, which are obtained by numerical integration. Additional information about the harmonic intensity can be extracted from the electron trajectory and its velocity along a quantum orbit. For example, because the ionization probability exponentially decreases with the square of the initial velocity, the most intense harmonics correspond to quantum orbits where the electron starts with the lowest velocities. The simple-man model, which treats the liberated electron classically, can be used to predict the position of the cutoff for different values of the relative phase and the crossing angle. Also, the regions with large harmonic intensity can be located using this model.

A very interesting and challenging result concerns the behavior of the harmonic ellipticity in the ω-2ω case, when the crossing angle approaches 90°. If the two field components are exactly perpendicular, the harmonics are linearly polarized. However, even the slightest deviation from exact perpendicularity (by as little as 0.1%) already produces significant elliptical polarization. A similarly astonishing effect was observed when the crossing angle remains perpendicular but the two linearly polarized driving-field components acquire an ever so slight ellipticity [44]. If this effect is genuine and not somehow an artifact of the strong-field approximation, it raises interesting questions. For example, to what extent can exact perpendicularity be guaranteed in an experiment? Since, moreover, the ellipticities calculated in the close vicinity of a 90° crossing angle rapidly fluctuate depending on the precise value of this angle on the same 0.1% scale, theoretical modeling of any given experiment requires very high precision. Discrepancies between experimental and theoretical results may easily be due to insufficient control of the crossing angle and/or the ellipticity of the driving-field components.

We described the two linearly polarized fields in the dipole approximation oscillating in time only. While their polarizations are noncollinear, they do not propagate. Fields that propagate in different directions offer distinct advantages for high-order harmonic generation. For example, two counterrotating circularly polarized fields of the same frequency and intensity whose propagation directions enclose a nonzero angle generate well-separated circularly polarized harmonics in the far field, each having a certain value of the helicity and the harmonic order [84,85]. To some extent, we can apply our results to such a case. Namely, in the focal region where the two driving fields are superimposed, the fact that they propagate in different directions hardly plays a role for the generation of harmonics. It is only after their generation that different harmonics separate and propagate in different directions. In the example of Refs. [84,85], the total field in the focus is linearly polarized in some direction (if the two counterpropagating fields have equal intensity), so the total harmonic field is linearly polarized as well. If this field is expanded in terms of circularly polarized waves of either helicity and each is assigned a different propagation direction, then the spectral shape observed in the experiment will approximately result.

In conclusion, two linearly polarized laser fields with an arbitrary angle between their polarizations and arbitrary frequencies can be successfully employed to generate elliptically polarized light. Particularly effective control of the HHG process is possible when both the crossing angle and the relative phase between the laser-field components are varied. The values of both angles can readily be controlled in an experiment. For the experimental realization and theoretical simulation of the ω-2ω frequency case, great care must be applied when the crossing angle approaches 90°. We hope that our results will stimulate experiments for the field configurations we suggested. In this case, more detailed simulations could be performed.

ACKNOWLEDGMENTS

We gratefully acknowledge support from the Ministry for Science, Higher Education and Youth, Canton Sarajevo, Bosnia and Herzegovina. We also acknowledge support from the Alexander von Humboldt Foundation.

[1] P. Salières, A. L'Huillier, Ph. Antoine, and M. Lewenstein, Study of the spatial and temporal coherence of high-order harmonics, Adv. At. Mol. Opt. Phys. **41**, 83 (1999).

[2] P. Tengdin, C. Gentry, A. Blonsky, D. Zusin, M. Gerrity, L. Hellbrück, M. Hofherr, J. Shaw, Y. Kvashnin, E. K. Delczeg-Czirjak *et al.*, Direct light-induced spin transfer between different elements in a spintronic Heusler material via femtosecond laser excitation, Sci. Adv. **6**, eaaz1100 (2020).

[3] T. D. Frazer, J. L. Knobloch, K. M. Hoogeboom-Pot, D. Nardi, W. Chao, R. W. Falcone, M. M. Murnane, H. C. Kapteyn, and J. N. Hernandez-Charpak, Engineering Nanoscale Thermal Transport: Size- and Spacing-Dependent Cooling of Nanostructures, Phys. Rev. Applied **11**, 024042 (2019).

[4] W. You, P. Tengdin, C. Chen, X. Shi, D. Zusin, Y. Zhang, C. Gentry, A. Blonsky, M. Keller, P. M.

Oppeneer *et al.*, Revealing the Nature of the Ultrafast Magnetic Phase Transition in Ni by Correlating Extreme Ultraviolet Magneto-Optic and Photoemission Spectroscopies, Phys. Rev. Lett. **121**, 077204 (2018).

[5] P. Tengdin, W. You, C. Chen, X. Shi, D. Zusin, Y. Zhang, C. Gentry, A. Blonsky, M. Keller, P. M. Oppeneer *et al.*, Critical behavior within 20 fs drives the out-of-equilibrium laser-induced magnetic phase transition in nickel, Sci. Adv. **4**, eaap9744 (2018).

[6] F. Brizuela, I. D. Howlett, S. Carbajo, D. Peterson, A. Sakdinawat, L. Yanwei, D. T. Attwood, M. C. Marconi, J. J. Rocca, and C. S. Menoni, Imaging at the nanoscale with practical table-top EUV laser-based full-field microscopes, IEEE J. Sel. Top. Quantum Electron. **18**, 434 (2012).

[7] M. D. Seaberg, D. E. Adams, E. L. Townsend, D. A. Raymondson, W. F. Schlotter, Y. Liu, C. S. Menoni, L. Rong, C.-C. Chen, J. Miao *et al.*, Ultrahigh 22 nm resolution coherent diffractive imaging using a desktop 13 nm high harmonic source, Opt. Express **19**, 22470 (2011).

[8] A. Ravasio, D. Gauthier, F. R. N. C. Maia, M. Billon, J.-P. Caumes, D. Garzella, M. Géléoc, O. Gobert, J.-F. Hergott, A.-M. Pena *et al.*, Single-Shot Diffractive Imaging with a Table-Top Femtosecond Soft X-Ray Laser-Harmonics Source, Phys. Rev. Lett. **103**, 028104 (2009).

[9] K. H. Lee, S. B. Park, H. Singhal, and C. H. Nam, Ultrafast direct imaging using a single high harmonic burst, Opt. Lett. **38**, 1253 (2013).

[10] N. Böwering, T. Lischke, B. Schmidtke, N. Müller, T. Khalil, and U. Heinzmann, Asymmetry in Photoelectron Emission from Chiral Molecules Induced by Circularly Polarized Light, Phys. Rev. Lett. **86**, 1187 (2001).

[11] U. Hergenhahn, E. E. Rennie, O. Kugeler, S. Marburger, T. Lischke, I. Powis, and G. Garcia, Photoelectron circular dichroism in core level ionization of randomly oriented pure enantiomers of the chiral molecule camphor, J. Chem. Phys. **120**, 4553 (2004).

[12] A. Ferré, C. Handschin, M. Dumergue, F. Burgy, A. Comby, D. Descamps, B. Fabre, G. A. Garcia, R. Géneaux, L. Merceron *et al.*, A table-top ultrashort light source in the extreme ultraviolet for circular dichroism experiments, Nat. Photon. **9**, 93 (2015).

[13] P. V. Demekhin, A. N. Artemyev, A. Kastner, and T. Baumert, Photoelectron Circular Dichroism with Two Overlapping Laser Pulses of Carrier Frequencies ω and 2ω Linearly Polarized in Two Mutually Orthogonal Directions, Phys. Rev. Lett. **121**, 253201 (2018).

[14] R. Cireasa, A. E. Boguslavskiy, B. Pons, M. C. H. Wong, D. Descamps, S. Petit, H. Ruf, N. Thire, A. Ferre, J. Suarez *et al.*, Probing molecular chirality on a sub-femtosecond time scale, Nat. Phys. **11**, 654 (2015).

[15] D. Ayuso, A. F. Ordonez, P. Decleva, M. Ivanov, and O. Smirnova, Strong chiral response in non-collinear high harmonic generation driven by purely electric-dipole interactions, Opt. Express **30**, 4659 (2022).

[16] S. Long, W. Becker, and J. K. McIver, Model calculations of polarization-dependent two-color high-harmonic generation, Phys. Rev. A **52**, 2262 (1995).

[17] H. Eichmann, A. Egbert, S. Nolte, C. Momma, B. Wellegehausen, W. Becker, S. Long, and J. K. McIver, Polarization-dependent high-order two-color mixing, Phys. Rev. A **51**, R3414 (1995).

[18] M. D. Perry and J. K. Crane, High-order harmonic emission from mixed fields, Phys. Rev. A **48**, R4051 (1993).

[19] S. Watanabe, K. Kondo, Y. Nabekawa, A. Sagisaka, and Y. Kobayashi, Two-Color Phase Control in Tunneling Ionization and Harmonic Generation by a Strong Laser Field and Its Third Harmonic, Phys. Rev. Lett. **73**, 2692 (1994).

[20] I. J. Kim, C. M. Kim, H. T. Kim, G. H. Lee, Y. S. Lee, J. Y. Park, D. J. Cho, and C. H. Nam, Highly Efficient High-Harmonic Generation in an Orthogonally Polarized Two-Color Laser Field, Phys. Rev. Lett. **94**, 243901 (2005).

[21] C. M. Kim, I. J. Kim, and C. H. Nam, Generation of a strong attosecond pulse train with an orthogonally polarized two-color laser field, Phys. Rev. A **72**, 033817 (2005).

[22] C. M. Kim and C. H. Nam, Selection of an electron path of high-order harmonic generation in a two-colour femtosecond laser field, J. Phys. B **39**, 3199 (2006).

[23] C. Ruiz, D. J. Hoffmann, R. Torres, L. E. Chipperfield, and J. P. Marangos, Control of the polarization of attosecond pulses using a two-color field, New J. Phys. **11**, 113045 (2009).

[24] L. Brugnera, F. Frank, D. J. Hoffmann, R. Torres, T. Siegel, J. G. Underwood, E. Springate, C. Froud, E. I. C. Turcu, J. W. G. Tisch *et al.*, Enhancement of high harmonics generated by field steering of electrons in a two-color orthogonally polarized laser field, Opt. Lett. **35**, 3994 (2010).

[25] H. Niikura, N. Dudovich, D. M. Villeneuve, and P. B. Corkum, Mapping Molecular Orbital Symmetry on High-Order Harmonic Generation Spectrum Using Two-Color Laser Fields, Phys. Rev. Lett. **105**, 053003 (2010).

[26] J. J. Xu, Isolated short attosecond pulse generation in an orthogonally polarized multicycle chirped laser field, Phys. Rev. A **83**, 033823 (2011).

[27] T. S. Sarantseva, M. V. Frolov, N. L. Manakov, M. Yu. Ivanov, and A. F. Starace, Harmonic generation spectroscopy with a two-colour laser field having orthogonal linear polarizations, J. Phys. B **46**, 231001 (2013).

[28] M. V. Frolov, N. L. Manakov, T. S. Sarantseva, A. A. Silaev, N. V. Vvedenskii, and A. F. Starace, Control of threshold enhancements in harmonic generation by atoms in a two-color laser field with orthogonal polarizations, Phys. Rev. A **93**, 023430 (2016).

[29] A. S. Emelina, M. Y. Emelin, R. A. Ganeev, M. Suzuki, H. Kuroda, and V. V. Strelkov, Two-color high-harmonic generation in plasmas: Efficiency dependence on the generating particle properties, Opt. Express **24**, 13971 (2016).

[30] G. Li, Y. Zheng, X. Ge, Z. Zeng, and R. Li, Frequency modulation of high-order harmonic generation in an orthogonally polarized two-color laser field, Opt. Express **24**, 18685 (2016).

[31] X. Liu, X. Zhu, L. Li, Y. Li, Q. Zhang, P. Lan, and P. Lu, Selection rules of high-order-harmonic generation: Symmetries of molecules and laser fields, Phys. Rev. A **94**, 033410 (2016).

[32] M. Murakami, O. Korobkin, and M. Horbatsch, High-harmonic generation from hydrogen atoms driven by two-color mutually orthogonal laser fields, Phys. Rev. A **88**, 063419 (2013); High-harmonic generation from hydrogen atoms driven by two-color mutually orthogonal laser fields, **95**, 059909(E) (2017).

[33] B. Zhang and M. Lein, High-order harmonic generation from diatomic molecules in an orthogonally polarized two-color laser field, Phys. Rev. A **100**, 043401 (2019).

[34] M. Murakami, O. Korobkin, and G.-P. Zhang, Time-dependent density-functional theory of high-order harmonic generation

from noble-gas atoms driven by orthogonally polarized two-color laser fields, Phys. Rev. A **101**, 063413 (2020).

[35] T. S. Sarantseva, M. V. Frolov, N. L. Manakov, A. A. Silaev, A. A. Romanov, N. V. Vvedenskii, and A. F. Starace, Attosecond-pulse metrology based on high-order harmonic generation, Phys. Rev. A **101**, 013402 (2020).

[36] G. S. Boltaev, M. Iqbal, N. A. Abbasi, V. V. Kim, R. A. Ganeev, and A. S. Alnaser, Enhanced XUV harmonics generation from diatomic gases using two orthogonally polarized laser fields, Sci. Rep. **11**, 5534 (2021).

[37] Y. Yang, L. Liu, J. Zhao, Y. Tu, J. Liu, and Z. Zhao, Effect of ionization asymmetry on high harmonic generation from oriented CO in orthogonal two-color fields, J. Phys. B **54**, 144009 (2021).

[38] W. Li and F. He, Generation and application of a polarization-skewed attosecond pulse train, Phys. Rev. A **104**, 063114 (2021).

[39] S. M. Njoroge, H. Yuan, K. Dickson, Q. Zhang, and P. Lan, Control of the polarization direction of isolated attosecond pulses using inhomogeneous two-color fields, Sci. Rep. **9**, 18582 (2019).

[40] A. J. Uzan, H. Soifer, O. Pedatzur, A. Clergerie, S. Larroque, B. D. Bruner, B. Pons, M. Ivanov, O. Smirnova, and N. Dudovich, Spatial molecular interferometry via multidimensional high-harmonic spectroscopy, Nat. Photon. **14**, 188 (2020).

[41] Y. Fang, C. He, M. Han, P. Ge, X. Yu, X. Ma, Y. Deng, and Y. Liu, Strong-field ionization of Ar atoms with a 45° cross-linearly-polarized two-color laser field, Phys. Rev. A **100**, 013414 (2019).

[42] C. Zhai, R. Shao, P. Lan, B. Wang, Y. Zhang, H. Yuan, S. M. Njoroge, L. He, and P. Lu, Ellipticity control of high-order harmonic generation with nearly orthogonal two-color laser fields, Phys. Rev. A **101**, 053407 (2020).

[43] Y. Fang and Y. Liu, Optimal control over high-order-harmonic ellipticity in two-color cross-linearly-polarized laser fields, Phys. Rev. A **103**, 033116 (2021).

[44] D. B. Milošević and W. Becker, High-order harmonic generation by bi-elliptical orthogonally polarized two-color fields, Phys. Rev. A **102**, 023107 (2020).

[45] A. Weber, B. Böning, B. Minneker, and S. Fritzsche, Generation of elliptically polarized high-order harmonic radiation with bi-elliptical two-color laser beams, Phys. Rev. A **104**, 063118 (2021).

[46] E. Bordo, O. Neufeld, O. Kfir, A. Fleischer, and O. Cohen, Spectroscopy of atomic orbital sizes using bi-elliptical high-order harmonic generation, Phys. Rev. A **100**, 043419 (2019).

[47] M. M. Hossain and H. Sakai, All-optical orientation of linear molecules with combined linearly and elliptically polarized two-color laser fields, J. Chem. Phys. **153**, 104102 (2020).

[48] X. Sun, D. Martinez, P. Froß, N. Camus, Y. Mi, W. Zhang, Z. Chen, T. Pfeifer, and R. Moshammer, Subcycle control of the photoelectron angular distribution using two-color laser fields having different kinds of polarization, Phys. Rev. A **103**, 033106 (2021).

[49] E. Bordo, O. Kfir, S. Zayko, O. Neufeld, A. Fleischer, C. Ropers, and O. Cohen, Interlocked attosecond pulse trains in slightly bi-elliptical high harmonic generation, J. Phys. Photon. **2**, 034005 (2020).

[50] A. Fleischer, O. Kfir, T. Diskin, P. Sidorenko, and O. Cohen, Spin angular momentum and tunable polarization in high-harmonic generation, Nat. Photon. **8**, 543 (2014).

[51] D. B. Milošević, Generation of elliptically polarized attosecond pulse trains, Opt. Lett. **40**, 2381 (2015).

[52] D. B. Milošević, High-order harmonic generation by a bichromatic elliptically polarized field: Conservation of angular momentum, J. Phys. B **48**, 171001 (2015).

[53] D. B. Milošević, Circularly polarized high harmonics generated by a bicircular field from inert atomic gases in the p state: A tool for exploring chirality-sensitive processes, Phys. Rev. A **92**, 043827 (2015).

[54] D. B. Milošević and W. Becker, X-ray harmonic generation by orthogonally polarized two-color fields: Spectral shape and polarization, Phys. Rev. A **100**, 031401(R) (2019).

[55] D. B. Milošević and W. Becker, Generation of elliptically polarized soft x rays using high-order harmonic generation with orthogonal two-color laser fields, J. Phys.: Conf. Ser. **1508**, 012001 (2020).

[56] D. Habibović, W. Becker, and D. B. Milošević, Attosecond pulse trains with elliptical polarization from an orthogonally polarized two-color field, J. Opt. Soc. Am. B **38**, 3367 (2021).

[57] D. Habibović, W. Becker, and D. B. Milošević, Symmetries and selection rules of the spectra of photoelectrons and high-order harmonics generated by field-driven atoms and molecules, Symmetry **13**, 1566 (2021).

[58] O. Neufeld, D. Podolsky, and O. Cohen, Floquet group theory and its application to selection rules in harmonic generation, Nat. Commun. **10**, 405 (2019).

[59] M. V. Frolov, N. L. Manakov, A. A. Minina, A. A. Silaev, N. V. Vvedenskii, M. Yu. Ivanov, and A. F. Starace, Analytic description of high-order harmonic generation in the adiabatic limit with application to an initial s state in an intense bicircular laser pulse, Phys. Rev. A **99**, 053403 (2019).

[60] A. V. Flegel, N. L. Manakov, I. V. Breev, and M. V. Frolov, Adiabatic expressions for the wave function of an electron in a finite-range potential and an intense low-frequency laser pulse, Phys. Rev. A **104**, 033109 (2021).

[61] D. B. Milošević and F. Ehlotzky, Scattering and reaction processes in powerful laser fields, Adv. At. Mol. Opt. Phys. **49**, 373 (2003).

[62] D. B. Milošević, W. Becker, and R. Kopold, Generation of circularly polarized high-order harmonics by two-color coplanar field mixing, Phys. Rev. A **61**, 063403 (2000).

[63] A. A. Radzig and B. M. Smirnov, *Reference Data on Atoms, Molecules and Ions* (Springer, Berlin, 1985).

[64] D. B. Milošević, G. G. Paulus, D. Bauer, and W. Becker, Above-threshold ionization by few-cycle pulses, J. Phys. B **39**, R203 (2006).

[65] D. B. Milošević, Macroscopic effects in high-order harmonic generation – a focal-averaging method based on the integral solution of the wave equation, Opt. Express **30**, 12163 (2022).

[66] A. A. Romanov, A. A. Silaev, T. S. Sarantseva, M. V. Frolov, and N. V. Vvedenskii, Study of high-order harmonic generation in xenon based on time-dependent density-functional theory, New J. Phys. **23**, 043014 (2021).

[67] A. W. Bray, D. Freeman, F. Naseem, V. K. Dolmatov, and A. S. Kheifets, Correlation-enhanced high-order-harmonic-generation spectra of Mn and Mn^+, Phys. Rev. A **101**, 053415 (2020).

[68] A. A. Romanov, A. A. Silaev, M. V. Frolov, and N. V. Vvedenskii, Influence of the polarization of a multielectron atom in a strong laser field on high-order harmonic generation, Phys. Rev. A **101**, 013435 (2020).

[69] R. Kopold, D. B. Milošević, and W. Becker, Rescattering Processes for Elliptical Polarization: A Quantum Trajectory Analysis, Phys. Rev. Lett. **84**, 3831 (2000).

[70] P. Salières, B. Carré, L. Le Déroff, F. Grasbon, G. G. Paulus, H. Walther, R. Kopold, W. Becker, D. B. Milošević, A. Sanpera *et al.*, Feynman's path-integral approach for intense-laser-atom interactions, Science **292**, 902 (2001).

[71] W. Becker, F. Grasbon, R. Kopold, D. B. Milošević, G. G. Paulus, and H. Walther, Above-threshold ionization: From classical features to quantum effects, Adv. At. Mol. Opt. Phys. **48**, 35 (2002).

[72] D. B. Milošević, Quantum-orbit analysis of high-order harmonic generation by bicircular field, J. Mod. Opt. **66**, 47 (2019).

[73] T. F. Gallagher, Above-Threshold Ionization in Low-Frequency Limit, Phys. Rev. Lett. **61**, 2304 (1988).

[74] P. B. Corkum, N. H. Burnett, and F. Brunel, Above-Threshold Ionization in the Long-Wavelength Limit, Phys. Rev. Lett. **62**, 1259 (1989).

[75] P. B. Corkum, Plasma Perspective on Strong Field Multiphoton Ionization, Phys. Rev. Lett. **71**, 1994 (1993).

[76] K. J. Schafer, B. Yang, L. F. DiMauro, and K. C. Kulander, Above Threshold Ionization Beyond the High Harmonic Cutoff, Phys. Rev. Lett. **70**, 1599 (1993).

[77] S. V. Popruzhenko, Keldysh theory of strong field ionization: History, applications, difficulties and perspectives, J. Phys. B **47**, 204001 (2014).

[78] D. B. Milošević and B. Piraux, High-order harmonic generation in a bichromatic elliptically polarized laser field, Phys. Rev. A **54**, 1522 (1996).

[79] C. Figueira de Morisson Faria, D. B. Milošević, and G. G. Paulus, Phase-dependent effects in bichromatic high-order harmonic generation, Phys. Rev. A **61**, 063415 (2000).

[80] D. Habibović, W. Becker, and D. B. Milošević, Ellipticity of high-order harmonics generated by aligned homonuclear diatomic molecules exposed to an orthogonal two-color laser field, Photonics **7**, 110 (2020).

[81] D. Habibović, W. Becker, and D. B. Milošević, High-order harmonic generation by aligned heteronuclear diatomic molecules in an orthogonally polarized two-color laser field, Eur. Phys. J. D **75**, 122 (2021).

[82] D. B. Milošević and W. Becker, Role of long quantum orbits in high-order harmonic generation, Phys. Rev. A **66**, 063417 (2002).

[83] M. V. Frolov, N. L. Manakov, A. A. Minina, N. V. Vvedenskii, A. A. Silaev, M. Yu. Ivanov, and A. F. Starace, Control of Harmonic Generation by the Time Delay Between Two-Color, Bicircular Few-Cycle Mid-IR Laser Pulses, Phys. Rev. Lett. **120**, 263203 (2018).

[84] D. D. Hickstein, F. J. Dollar, P. Grychtol, J. E. Ellis, R. Knut, C. Hernández-García, D. Zusin, C. Gentry, J. M. Shaw, T. Fan *et al.*, Non-collinear generation of angularly isolated circularly polarized harmonics, Nat. Photon. **9**, 743 (2015).

[85] J. L. Ellis, K. M. Dorney, C. G. Durfee, C. Hernández-García, F. Dollar, C. A. Mancuso, T. Fan, D. Zusin, C. Gentry, P. Grychtol *et al.*, Phase matching of noncollinear sum and difference frequency high harmonic generation above and below the critical ionization level, Opt. Express **25**, 10126 (2017).